Author Manuscript

Author Manuscript

Author Manuscript

Author Manuscript

HHS Public Access

Author manuscript

*Nat Chem Biol*. Author manuscript; available in PMC 2017 April 17.

Published in final edited form as:

*Nat Chem Biol*. 2016 December ; 12(12): 1075–1083. doi:10.1038/nchembio.2204.

# Identification and characterization of PPARα ligands in the hippocampus

**Avik Roy**[1], **Madhuchhanda Kundu**[1], **Malabendu Jana**[1], **Rama K. Mishra**[2], **Yeni Yung**[3], **Chi-Hao Luan**[4], **Frank J. Gonzalez**[5], and **Kalipada Pahan**[1,6]

[1]Department of Neurological Sciences, Rush University Medical Center, Chicago, IL

[2]Medicinal and Synthetic Chemistry Core, Center for Molecular Innovation and Drug Discovery, Northwestern University, Evanston, IL

[3]Research Resources Center, University of Illinois at Chicago, IL

[4]High Throughput Analysis Laboratory and Department of Molecular Biosciences, Northwestern University, Evanston, IL

[5]Laboratory of Metabolism, Center for Cancer Research, National Cancer Institute, National Institutes of Health, Bethesda, MD

[6]Division of Research and Development, Jesse Brown Veterans Affairs Medical Center, 820 South Damen Avenue, Chicago, IL

## Abstract

Peroxisome proliferator-activated receptor alpha (PPARα) regulates hepatic fatty acid catabolism and mediates the metabolic response to starvation. Recently, we have found that PPARα is constitutively activated in nuclei of hippocampal neurons and controls plasticity via direct transcriptional activation of CREB. Here, three endogenous ligands of PPARα, 3-hydroxy-(2,2)-dimethyl butyrate, hexadecanamide, and 9-octadecenamide were discovered in mouse brain hippocampus. Mass spectrometric detection of these compounds in mouse hippocampal nuclear extracts, *in silico* interaction studies, time-resolved FRET analyses, and thermal shift assay clearly indicated that these three compounds served as ligands of PPARα. Site-directed mutagenesis studies further revealed that PPARα Tyr 464 and Tyr 314 were involved in binding these hippocampal ligands. Moreover, these ligands activated PPARα and upregulated synaptic function of hippocampal neurons. These results highlight the discovery of hippocampal ligands of PPARα capable of modulating synaptic functions.

Users may view, print, copy, and download text and data-mine the content in such documents, for the purposes of academic research, subject always to the full Conditions of use: http://www.nature.com/authors/editorial_policies/license.html#terms

To whom correspondence should be addressed: Kalipada Pahan, Ph.D., Department of Neurological Sciences, Rush University Medical Center, 1735 West Harrison St, Suite 310, Chicago, IL 60612, Telephone (312) 563-3592; Fax (312) 563-3571, Kalipada_Pahan@rush.edu.

**Author contributions**

A.R. and K.P. designed the study. A.R., M.K. and M.J. performed most of the experiments. Y.Y. performed GC-MS. R.K.M. performed *in-silico* structural analysis. C.H. L. performed TR-FRET analysis. A.R., F.J.G. and K.P. wrote the manuscript.

**Competing financial interests**

None

Author Manuscript Author Manuscript Author Manuscript Author Manuscript

## Introduction

Peroxisome proliferator-activated receptor α (PPARα) belongs to a class of nuclear hormone receptors[1] that participates in a diverse range of biological functions including control of fatty acid transport and catabolism[2], anti-inflammation[3], immuno-modulation[4], and anti-oxidation[5]. However, recently we have shown that PPARα also plays an important role in the modulation of synaptic function in hippocampus via transcriptional upregulation of CREB[6–8]. It has been also delineated that activation of PPARα in hippocampal neurons leads to the increase in ADAM10 transcription and subsequent non-amyloidogenic proteolysis of APP[9]. These reports highlight a lipid-independent role of PPARα in controlling brain function. Otherwise, it was believed that the presence of peroxisomes could be important for the compensation of mitochondrial instability in the adult brain hippocampus[10].

Since interaction with ligand plays an instrumental role in modulating the biological effect of most nuclear hormone receptors[11] including PPARα, we were prompted to investigate the existence of endogenous ligands of PPARα in the hippocampus. Successful identification of endogenous modulators of PPARα would aid in understanding the endogenous regulation hippocampal function and memory by PPARα. However, little is known about the presence of endogenous ligands of PPARα in the hippocampus and their role in regulating the synaptic plasticity. Although endocannabinoid-like molecules including oleoylethanolamide[12,13] and palmitoylethanolamide[14], the fatty acid derivative 20-carboxy-arachidonic acid[15], and leukotriene B4[16] have been considered as endogenous PPARα ligands, these compounds are ubiquitously present in different tissues including liver[17], kidney[18] and brain[19]. Furthermore, these compounds display a wide range of biological activities starting form antioxidant, anti-inflammation to neuroprotection[14,18]. In an attempt to find an endogenous ligand for PPARα, a recent study[20] revealed that 1-palmitoyl-2-oleoyl-sn-glycerol-3-phosphocholine (16:0/18:1-GPC) could serve as a potent ligand of PPARα in liver. However, until now, nothing is known about the presence of endogenous ligand(s) in the hippocampus that are capable of modulating the PPARα activity in hippocampal neurons.

Because PPARα is constitutively present in nuclei of hippocampal neurons, ligands must be constitutively present in the hippocampal neurons as well. Therefore, in an attempt to isolate such ligands, we used GST-coupled PPARα ligand-binding domain (LBD) as a bait and identified three novel ligands [hexadecanamide (HEX), octadecenamide (OCT) and 3-hydroxy, 2, 2-dimethyl butyrate (HMB)] from hippocampal nuclear extracts. Interestingly, these hippocampal ligands bound to a region of the receptor requiring Tyr314 and Tyr464 residues in the ligand-binding pocket of PPARα to activate PPARα and stimulate synaptic function of hippocampal neurons.

## Results

### PPARα in the expression of plasticity-related genes

PPARα is strongly expressed in hippocampal neurons[6–8]. Since hippocampal neurons are equipped with a wide-spectrum of synaptic proteins related to long term potentiation

Author Manuscript Author Manuscript Author Manuscript Author Manuscript

(LTP)[21] and long term depression (LTD)[22], we examined the role of PPARα in regulating the expression of different LTP- and LTD-associated synaptic molecules. LTP causes a persistent increase in synaptic strength between pre- and post-synaptic neurons, whereas LTD causes a persistent reduction of synaptic strength. An mRNA-based microarray followed by heat map analyses (Figure 1A) clearly revealed that hippocampus of *Ppara*-null (KO) mice displayed upregulation of 34 genes (Figure 1B & Supplementary Results, Supplementary Figure 1A), down-regulation of 26 genes (Figure 1B & Supplementary Figure 1B), and no alteration in 22 genes (Figure 1B). Most of the downregulated mRNAs are involved in LTP, including the ionotropic AMPA receptors *Gria1* and *Gria3* mRNAs; ionotropic NMDA receptors *Grin1*, *Grin2a* and *Grin2b* mRNAs; immediate early genes (IEGs) mRNAs including *Arc*, *Homer1* and *Fos*; and different synaptic membrane encoded mRNAs *Adam10*, *Dlg4*, *Synpo*, and *Adcy1* (Figure 1B & Supplementary Figure 1B). On the contrary, most of the upregulated mRNAs are associated with LTD including different protein phosphatase mRNAs such as *Ppp1ca, Ppp2ca, Ppp3ca; Ngfr*, *Pick1*, *Nos1*, and *Nfkb1* (Figure 1B & Supplementary Figure 1A). The downregulation of some crucial LTP-associated mRNAs in KO hippocampus including *Arc*, *Gria1*, *Grin2a*, *Grin2b*, and *Creb* was separately confirmed by real-time PCR analyses (Figure 1C). Immunohistochemical analyses of PSD-95 (encoded by the *Dlg4* gene) in the presynaptic fibers of CA1 hippocampus (Figure 1D & 1E) and immunoblot assay of NR2A (encoded by *Grin2a*), GluR1 (encoded by *Gria1*), PSD-95, Arc, and CREB (Figure 1F & 1G) further indicated that hippocampus of KO brain expressed less LTP-associated molecules than the hippocampus of WT mice.

## Identification of novel hippocampal ligands of PPARα

PPARs are nuclear receptors that require the binding of ligands for activation of gene expression. Immunostaining of hippocampal sections (Supplementary Figure 2A) and immunoblot analyses of nuclear-enriched fractions of hippocampal extracts (Supplementary Figure 2B–E) clearly demonstrated that PPARα, but neither PPARβ nor PPARγ, was present in nuclei. These results suggest that the hippocampus has endogenous expression of PPARα agonist and that such ligands should be present within the nucleus. In order to identify these ligands, we adopted gas chromatography-mass spectrometry (GC-MS). Briefly, nuclear extracts were prepared from mouse hippocampus, incubated with a GST-tagged PPARα ligand binding domain (LBD), purified with affinity chromatography, reconstituted with chloroform or acetonitrile, and GC-MS analyses performed (Figure 2A–C). Analysis of chloroform extracts displayed two distinct peaks matching 9-octadecenamide (OCT) with an m/z of 281.38 at 23.03 minute (Figure 2A) and hexadecanamide (HEX) with an m/z of 255.01 at 21.45 minute (Figure 2B). On the other hand, GC-MS analyses of the acetonitrile fraction of affinity purified hippocampal nuclear extract resulted a distinct peak of m/z 160.0 at 14.48 minutes that matched the NIST library for 3-hydroxy (2, 2)-dimethyl butyric acid ethyl ester (HMB) (Figure 2C). Interestingly, GC-MS analyses of hippocampal nuclear extracts after pulling down with PPARβ-LBD did not exhibit any peak (Figure 2D–E), suggesting that these three hippocampal ligands could be specific for PPARα. The fraction of hippocampal nuclear extracts eluted through the glutathione column was further immunoblotted to validate the accuracy of our affinity purification procedure, which clearly showed that all parameters including the amount of

Author Manuscript Author Manuscript Author Manuscript Author Manuscript

hippocampal tissue, amount of recombinant protein, and the volume of eluate were kept constant in all cases throughout the assay (Figure 2F). However, our above-mentioned assay was unable to demonstrate if these ligands could display similar interaction with *de novo*-synthesized PPARα. Therefore, next, we infected cultured *Ppara*-null hippocampal neurons with lentiviral particles containing full-length PPARα (*lenti-FL-Ppara*) and then performed immunoprecipitation followed by GC-MS (Figure 2G–H). Similar to our previous observations, both OCT and HEX were found to be bound to *de novo*-synthesized PPARα in *lenti-FL-Ppara*-transduced (Figure 2H), but not with empty lenti-vector-transduced, *Ppara*-null neurons (Figure 2G). The efficiency of gene transduction was measured by immunoblot analyses of cell extract with PPARα antibody (Figure 2I). In addition, our analyses successfully identified a group of biological ligands of PPARα, which are endogenously produced in the hippocampus. Some of these detected compounds are sulfur-containing unknown compounds such as thiazoles (MW 220–240), thiosemicarbazones (MW 190–200) and thiazolidine esters (MW 250–270) (Supplementary Table 1). However, these compounds were excluded from this study because of their unknown biosynthetic pathway, relatively poor match-factor (<65), and commercial unavailability. Trans-O-dithiane-4, 5 diol is the oxidized product of DTT used in the buffer whereas D-galactono 1, 4-lactone 5, 6-octylidene is excluded because of the commercial unavailability of this compound required to confirm its association with PPARα. Taken together, our GC-MS analyses identified OCT, HEX and HMB as three putative, endogenously produced, but also commercially available, PPARα ligands. Next, Time Resolved-Fluorescence Resonance Energy Transfer (TR-FRET) assay was performed to confirm the interaction between these ligands and PPARα. Optimized TR-FRET analysis[7] (Figure 3A–C) indicated that PGC1α-PPARα LBD complex displayed a strong interaction with all these three ligands (Figure 3A–C). In all cases, TR-FRET signals (Figure 3A–C) released by the PPARα LBD showed a steady increase. Although the signal intensity was observed higher in HMB compared to OCT (Figure 3A) and HEX (Figure 3B), both OCT and HEX generated FRET signals at much lower concentrations than that of HMB. On the other hand, we observed a large thermal shift as evidenced by a change in melting temperature of purified PPARα-LBD protein when incubated with these ligands (Figure 3D–F), suggesting that these ligands truly interact with the ligand binding domain of PPARα with high efficiency.

## Interaction between PPARα and its novel ligands

Next, we characterized the molecular interaction of these ligands with the PPARα LBD. Our *in silico* computer-aided cheminformatics analyses generated a reasonable docked pose of these ligands in the PPARα LBD (Figure 3G–I). The docked pose of all three ligands showed two potential hydrogen bonds between the ligand and two active-site residues, Tyr314 (Y314) and Tyr464 (Y464) of the PPARα-LBD. The ligand-binding surface is amphipathic, as it shared both a negatively charged electrostatic surface and a few patches of a partial positively charged surface with mostly lipophilic (brown), and some hydrophilic patches (blue) (Supplementary Figure 3A & 3B). Imposing the most stringent docking protocols, a reasonable docked poses of OCT (a total score of 10.15, a polar score of 1.05, and a crash score of −1.49; total binding energy −25.56 kcal/mol), HEX (a total score of 10.0, a polar score of 1.81, and a crash score of −1.04; total binding energy −26.3 kcal/mol), and HMB (a total score of 5.63, a polar score of 1.93, and a crash score of −1.55; total

Author Manuscript Author Manuscript Author Manuscript Author Manuscript

binding energy −10.5 kcal/mol) were obtained for PPARα. Interestingly, in the case of both PPARβ and PPARγ, by applying similar docking protocols, we failed to obtain any docked pose for these ligands, suggesting that the interaction of all three ligands with PPARα-LBD is specific and not possible in other PPAR isoforms. To further confirm our observation, we performed in silico mutation analysis, in which OCT, HEX, and HMB were placed in the ligand-binding pocket of Y464D/Y314D-PPARα. After energy minimization (total binding energy is −15.6 kcal/mol for OCT, −14.3 kcal/mol for HEX and −5.04 kcal/mol for HMB), all three ligands were observed to be located far (>4A°) from either D464 or D314 residue to establish any hydrogen bond (Figure 4A–C), suggesting that the mutation of tyrosine 464 to aspartate significantly impairs the interaction of these ligands with PPARα. However, *in silico* modeling of protein-ligand interaction is hypothetical and requires rigorous experimental analysis for further validation.

Therefore, next, lentivirus-mediated *de novo* expression studies were performed, where we over-expressed wild-type full-length (*GFP-FL-Ppara*) and three different LBD-mutated PPARα (*GFP-Y314D*, *GFP-Y464D* and *GFP-Y314D/Y464D*) recombinant proteins (Supplementary Figure 4A) in neurons followed by binding analyses with three endogenous ligands. Briefly, site-directed mutagenesis was performed in the mouse PPARα with Y314 and Y464 residues replaced separately or together with aspartate (D). After that, the entire mouse *GFP-Ppara* gene (*GFP-FL-Ppara*) and three different mutated genes were cloned in the pLenti6/V5-TOPO lentiviral expression vector, packaged in lentivirus particle with HEK293FT cells, purified full-length and mutated PPARα proteins in a GFP-affinity column, and finally thermal shift assays were performed in order to analyze their conformational stability. Both full length (Figure 4D) and mutated (Figure 4E) proteins displayed a similar pattern of thermal shift with equivalent melting temperature (Tm), suggesting that mutations in Y314 and Y464 residues did not alter the conformational stability of PPARα. Moreover, OCT, HEX and HMB did not alter the Tm in Y464D-PPARα, demonstrating that mutation of tyrosine 464 to aspartate significantly impacted the binding of these ligands to the LBD of PPARα (Figure 4F). In another experiment, *Ppara*-null hippocampal neurons were transduced with different lentiviral PPARα constructs and transduction efficiencies were basically the same in all cases (Supplementary Figure 5A) and the level of PPARα was comparable in cells transduced with different constructs (Supplementary Figure 5B–C). After 48 h of transduction, the cells were homogenized, passed through the GFP-affinity column, eluted, fractionated with chloroform-methanol, and finally analyzed by GC-MS for the detection of ligands. Interestingly, we observed that the affinity-purified nuclear extract of *lenti-GFP-FL-Ppara*- (Supplementary Figure 4B), but not *lenti-GFP*- (Supplementary Figure 4C), transduced *Ppara*-null neurons contained these ligands. Interestingly, the mutation of Y314 was found to partially impact the ligand binding affinity of PPARα as we detected low amount of both OCT and HEX in the nuclear extract of *lenti-GFP-Y134D-Ppara*-transduced *Ppara*-null neurons (Figure 4G). On the other hand, mutation of the Y464 completely knocked down the ligand binding affinity as we observed profound loss of ligand binding in both *lenti-GFP-Y464D-Ppara*- (Figure 4H) and *lenti-GFP-Y314D/Y464D-Ppara*- (Figure 4I) transduced *Ppara*-null neurons. Throughout these analyses, we used 2, 4-bis (α, α-dimethyl benzyl) phenol as an internal standard (Supplementary Figure 6A–F). We normalized peak area of different ligands with that of

Author Manuscript Author Manuscript Author Manuscript Author Manuscript

internal standard and then quantified the binding affinity of these ligands with different construct of PPARα by peak integration statistics (Supplementary Table 2). Taken together, our detailed GC-MS analyses clearly indicated that both Y314 and Y464 residues of the PPARα-LBD were crucial for its interaction with endogenous ligands.

Next, we monitored the role of these ligands in controlling the transcriptional activity of PPARα. First, we performed PPRE-driven luciferase assay in cultured astrocytes treated with different concentrations of HEX (Figure 5A), OCT (Figure 5B), and HMB (Figure 5C). We observed that all three ligands increased the PPRE-luciferase activity in a dose-dependent manner (Figure 5A–C). However, PPRE-luciferase gene (*tk-PPREx3-Luc*)-transfected astrocytes displayed significant level of cytotoxicity with higher concentrations of HEX (Supplementary Figure 7A), OCT (Supplementary Figure 7B) and HMB (Supplementary Figure 7C), justifying the decrease of PPRE-luciferase activity with higher doses of ligands (Figure 5A–C). Consistent to our TR-FRET assay, both OCT and HEX increased PPRE-luciferase activity at much lower concentration as compared to HMB (Figure 5A–C). Similarly, these ligands were also able to induce PPRE-luciferase activity in *Ppara*-null astrocytes transduced with *lenti-FL-Ppara*, but not *lenti-vector* (Figure 5D–E).

To further confirm the specificity of these ligands to PPARα, we performed PPRE-luciferase assay in PPARβ KO (*Pparb*-null) astrocytes. These astrocytes were pre-treated with PPARγ-antagonist GW9662 to nullify the involvement of PPARγ in reporter assay. Inhibition of rosiglitazone-mediated increase in PPRE-luciferase activity by GW9662 (Supplementary Figure 8A) suggests that this inhibitor is capable of suppressing the function of PPARγ in *Pparb*-null astrocytes. OCT (Supplementary Figure 8B), HEX (Supplementary Figure 8C) and HMB (Supplementary Figure 8D) markedly increased PPRE luciferase activity in *Pparb*-null astrocytes. Interestingly, GW9662 remained unable to inhibit OCT-, HEX- and HMB-mediated increase in PPRE-luciferase activity in *Pparb*-null astrocytes (Supplementary Figure 8B–D), indicating the specificity of these ligands towards PPARα. To further confirm this finding, we performed ChIP analyses of the CREB promoter (Supplementary Figure 8E) as described recently[6] and observed that all three ligands stimulated the recruitment of PPARα and its coactivator PGC1α to the CREB promoter (Supplementary Figure 8F–H). Since Y314 and Y464 residues of PPARα-LBD were crucial for the interaction with hippocampal ligands, we examined whether these residues were also involved in hippocampal ligand-mediated activation of PPARα. As expected, HEX, OCT and HMB remained unable to induce PPRE-driven luciferase activity in *Ppara*-null astrocytes (Figure 5D). However, all three ligands markedly induced PPRE reporter activity in *Ppara*-null astrocytes that were transduced with lentivirions containing *FL-Ppara* (Figure 5E). On the other hand, Y314D mutation in PPARα-LBD displayed partial induction of PPRE-luciferase activity (Figure 5F) as we observed in our GC-MS analysis that the interaction of all three ligands was partially compromised with Y314D PPARα. Consistent to GC-MS results, all three ligands were unable to stimulate PPRE-luciferase activity in *Ppara*-null astrocytes infected with lentiviruses containing either *Y464D-Ppara* (Figure 5G) or *Y314D/Y464D-Ppara* (Figure 5H), suggesting that the Y464D mutation is sufficient to knockdown PPARα activation by its endogenous hippocampal ligands. Commercial ligands of PPARα (WY14643, fenofibrate and clofibrate) were also unable to induce PPRE-luciferase activity in *Ppara*-null astrocytes (Figure 5I). However, these commercial ligands

Author Manuscript Author Manuscript Author Manuscript Author Manuscript

markedly induced PPRE-luciferase activity in *Ppara*-null astrocytes that were transduced with *lenti-FL-Ppara* (Figure 5J). On the other hand, commercial ligands of PPARα displayed no luciferase activity when *Ppara*-null astrocytes were transduced with *lenti-Y314D-Ppara* (Figure 5K), *lenti-Y464D-Ppara* (Figure 5L), and *lenti-Y314D/Y464D-Ppara* (Figure 5M), suggesting that both Y314 and Y464 residues of PPARα are important for the binding with commercially available ligands. Similar to astrocytes, the transduction of either *lenti-Y464D-Ppara* or *lenti-Y314D/Y464D-Ppara*, but neither *lenti-FL-Ppara* nor *lenti-Y314D-Ppara* (Supplementary Figure 9A–E), completely abrogated the PPRE-luciferase activity in OCT-, HEX-, and HMB-treated *Ppara*-null hippocampal neurons. Collectively, these results suggest a mandatory role for the Y464 residue and a partial role for the Y314 residue in the binding and activation of PPARα by endogenous hippocampal ligands.

## Modulation of synaptic function by hippocampal ligands

Next, we investigated whether these hippocampal ligands were capable of improving synaptic function of hippocampal neurons. Our immunoblot (Supplementary Figure 10A) followed by relative densitometric analyses (Supplementary Figure 10B–D) and immunofluorescence analyses of NR2A (Supplementary Figure 10E) and GluR1 (Supplementary Figure 10F) clearly demonstrated that HEX, OCT and HMB upregulated, NR2A, GluR1 and CREB in WT, but not *Ppara*-null, hippocampal neurons, suggesting that these ligands increased the expression of synaptic molecules via PPARα.

Dendritic spines are the crucial mediators of synaptic transmission among central neurons and often serve as a primary candidate for the long-term morphological substrates of neuronal plasticity[23,24]. Therefore, we investigated the effect of these ligands on the increase of spine density in cultured hippocampal neurons. Briefly, mouse *Ppara*-null hippocampal neurons were transduced with lentivirus containing empty vector, *FL-Ppara*, or *Y464D-Ppara* for a week followed by the treatment with OCT, HEX, and HMB for four more days. After that, neurons were labelled with phalloidin to monitor the spine density. Interestingly, the transduction of *Ppara*-null neurons with *lenti-Y464D-Ppara*, but not *lenti-FL-Ppara*, significantly attenuated the density of dendritic spines (Figure 6A). Moreover, treatment with OCT (Figure 6B), HEX (Figure 6C), HMB (Figure 6D), and the synthetic agonist WY14643 (Figure 6E) stimulated the density of spines only when *Ppara*-null neurons were transduced with *lenti-FL-Ppara*, but not *lenti-Y464D-Ppara*, further suggesting that the PPARα Y464 residue is crucial for the induction of morphological plasticity by its endogenous ligands. We further validated our observation by measuring the area of spine heads (Supplementary Figure 11A–B) and number of spines (Supplementary Figure 11C) in HEX-, OCT-, and HMB-treated *Ppara*-null neurons.

HEX (Supplementary Figure 10G–H), OCT (Supplementary Figure 10I–J) and HMB (Supplementary Figure 10K–L) stimulated the expression of CREB in *Ppara*-null hippocampal neurons that were transduced with lentivirions containing *FL-Ppara* gene. On the other hand, HEX, OCT and HMB remained unable to increase the expression of CREB in *Ppara*-null hippocampal neurons that were transduced with *lenti-Y464D-Ppara* and *lenti-Y464D/Y314D-Ppara* (Supplementary Figure 10G–L). Moreover, Y314D mutation only

Author Manuscript Author Manuscript Author Manuscript Author Manuscript

partially restored the expression of CREB in response to OCT, HEX and HMB in *lenti-Y314D-Ppara*-transduced *Ppara*-null neurons (Supplementary Figure 10G–L).

Calcium oscillation through metabotropic receptors has been implicated in synaptic plasticity and recently we have demonstrated that both AMPA and NMDA elicited much weaker calcium influx and a smaller amplitude oscillation in *Pparα*-null than WT hippocampal neurons[6]. Consistently, we have seen that HEX, OCT and HMB stimulated AMPA-mediated calcium influx in *lenti-FL-Ppara*-transduced *Ppara*-null hippocampal neurons (Figure 6F). While *lenti-Y314D-Ppara* was only able to partially restore HEX-, OCT- and HMB-elicited calcium influx in AMPA-treated *Ppara*-null hippocampal neurons (Figure 6G), these ligands remained unable to increase AMPA mediated calcium influx in *Ppara*-null hippocampal neurons that were transduced with either *lenti-Y464D-Ppara* (Figure 6H) or *lenti-Y314D/Y464D-Ppara* (Figure 6I). Similar results were seen for HEX, OCT and HMB in case of NMDA-mediated calcium influx in *lenti-FL-Ppara-*, *lenti-Y314D-Ppara-*, *lenti-Y464D-Ppara-,* and *lenti-Y314D/Y464D-Ppara*-transduced *Ppara*-null hippocampal neurons (Figure 6J–M). These results suggest pivotal role of Y464 residue and limited role of Y314 residue of PPARα in OCT-, HEX-, and HMB-stimulated calcium influx through NMDA and AMPA-sensitive receptors.

## Discussion

Since PPARα has been reported to be localized in the different parts of the brain[25] and might play crucial role in controlling different brain function[6,26], there is a growing interest in identifying the endogenous agonist for PPARα in this tissue. Although different studies speculated that anandamides or 9-olylethanolamide could serve as central ligands of PPARα[27], there is no experimental evidence that shows the molecular interaction between 9-oleoylethanolamide and PPARα; however 9-oleoylethanolamide was shown to display PPARα-independent effects[28]. Moreover, there are many structurally similar fatty-acyl amides available in the CNS that have not been evaluated as potential endogenous ligands of PPARα. Here, we delineate the isolation and characterization of three novel ligands of PPARα [octadecenamide (OCT), hexadecanamide (HEX), and 3-hydroxy-2,2-dimethyl butyrate (HMB)] from the hippocampus. *First*, GC-MS analyses of PPARα LBD-pulled down fraction of hippocampal nuclear extract revealed the existence of these compounds. Interestingly, these three compounds were detected only in PPARα LBD-, but not PPARβ LBD-pulled down fraction of hippocampal nuclear extract, suggesting that these ligands are specific for PPARα. In addition to these three major ligands, we also detected some thionated compounds including thiazoles (*mw* 220–240), thiosemicarbazones (*mw* 190–200), and thiazolidine esters (*mw* 250–270) while performing GC-MS analyses. *Second*, de novo establishment of PPARα by lentiviral transduction of *Ppara* gene in Ppara-null hippocampal neurons followed by similar GC-MS analysis also resulted in the detection of these three ligands. *Third*, further characterization of these molecules by TR-FRET and thermal shift assay revealed that HEX, OCT and HMB strongly interacted with the LBD of PPARα. Our high-throughput studies indicated that all three ligands served as full ligands of PPARα as we observed the slope of the curve derived from both FRET and thermal-shift assay shifted along the positive direction of X axis. While measuring their affinity, EC50 values of these ligands ($EC50_{OCT}$ = 4.838 μM; $EC50_{HEX}$ = 5.264 μM; $EC50_{HMB}$ = 35.85

Author Manuscript Author Manuscript Author Manuscript Author Manuscript

μM) were observed higher than the same for GW7647 (EC50 = 5.961 nM), a pharmacological agonist of PPARα (Supplementary Figure 12). These results suggest that our newly discovered hippocampal ligands have less affinity compared to commercially available ligands.

Our *in silico* analysis, site-directed mutation of Y314 and Y464 residues of PPARα followed by lentiviral manipulation in *Ppara*-null hippocampal neurons revealed that both Y314 and Y464 residues of PPARα are involved in the interaction with these ligands, with the PPARα Y464 residue being more critical than the Y314 residue. This observation was further validated by analysis of the transcriptional activity of PPARα where Y464D mutation of PPARα did not restore PPRE-luciferase activity in OCT-, HEX-, and HMB-treated *Ppara*-null hippocampal neurons. Previous studies have reported the 9-oleylethanolamine could serve as a ligand for PPARα in the brain; however, we could not detect 9-oleylethanolamine in hippocampus by GC-MS after pulling down the hippocampal extracts with recombinant PPARα LBD. One possibility is that we have pulled down PPARα LBD only from the nuclear extracts and that 9-oleylethanolamine is not present in the nucleus. We targeted nuclear fraction of PPARα for its ligand detection as PPARα is constitutively present in nuclei of hippocampal neurons.

Recently, we have shown that PPARα regulates the transcription of CREB and controls the expression of CREB-associated synaptic genes[6]. In another study, we have described that statin-mediated nuclear activation of PPARα is also important to regulate the expression of neurotrophins in different brain cells[7]. Our detailed molecular interaction analyses reveal that statins interact with L331 and Y334 residues of PPARα LBD in the presence of PGC1α and controls the transcription of CREB. However, commercially available ligands and the endogenous ligands described in this study, do not interact with these two residues of PPARα. Instead, these molecules interact with Y314 and Y464 residues of the PPARα LBD.

Characterizing drugs for improving synaptic plasticity is an important area of research. Interestingly, these hippocampal ligands increased synaptic properties of hippocampal neurons. However, these compounds stimulated the expression of different synaptic molecules in WT, but not in *Ppara*-null neurons. Stimulation of dendritic spine formation and increase in NMDA- and AMPA-driven calcium influx by hippocampal ligands in *Ppara*-null hippocampal neurons upon establishment of *FL-Ppara*, but not *Y464D-Ppara*, indicates the importance of Y464 residue of PPARα in synaptic properties of hippocampal ligands. While Y464 residue of PPARα was fully responsible for the functioning of these ligands, Y314 residue was also partly involved in this process. Earlier studies suggest that OCT could be beneficial in controlling sleep as it has been found in the cerebrospinal fluid during sleep deprivation[29]. Since OCT and two other compounds HEX and HMB are constitutively present in the hippocampus as PPARα ligands, it would be interesting to see if these compounds increase sleep via PPARα.

Author Manuscript Author Manuscript Author Manuscript Author Manuscript

# Online methods

## Animals

Animal maintaining and experiments were in accordance with National Institute of Health guidelines and were approved by the Institutional Animal Care and Use committee of the Rush University of Medical Center, Chicago, IL. *Ppara*-null and their wild-type controls (C57/BL6J) were purchased from Jackson Laboratory. Mice were housed in ventilated micro-isolator cages in an environmentally controlled vivarium (7:00 A.M. /7:00P.M. light cycle; temperature maintained at 21–23°C; humidity 35–55%). Animals were provided standard mouse chow and water ad libitum and closely monitored for health and overall well-being daily by veterinary staff and the investigator.

## Reagents

Rabbit polyclonal anti-PPARα antibody (Abcam; Cat# ab189159; WB and IHC), mouse anti-NeuN antibody (Millipore; Cat# MAB377), rabbit polyclonal anti-PPARβ antibody (Abcam; Cat # ab8937; WB and IHC), anti-PPARγ antibody (Abcam; Cat# ab66343; WB and IHC), anti-NMDAR2A antibody (Cell Signaling for WB at a dilution of 1:1000, Cat #4205; Abcam for IHC, Cat# ab169873), anti-GluR1 antibody (Cell Signaling for WB at a dilution of 1:1000, Cat #13185; Abcam for IHC, Cat # ab131507), anti-CREB antibody ( Cell Signaling for WB at a dilution of 1:1000 and IC at a dilution of 1:200, Cat# 9104), and anti-Arc antibody (Abcam for WB at a dilution of 1:1000, Cat # ab118929) were used in this study. Different pharmacological compounds including 9-octadecenamide (Cat#O2136), hexadecanamide (Cat#S350435), 2,4-bis(α,α-dimethyl benzyl) phenol (Cat #372129), gemfibrozil (Cat #G9518), clofibrate (Cat# C6643), fenofibrate (Cat# F6020), GW9662 (Cat# M6191), WY-14643 (Cat# C7081), and MTT-based toxicity assay kit (Stock No. TOX-1) were purchased from Sigma-Aldrich. GST-PPARα-LBD and GST-PPARβ-LBD were purchased from Protein One. On the other hand, 3-hydroxy 2, 2-dimethyl butyric acid ethyl ester (Cat# sc-216452) was purchased from Santa Cruz.

## Isolation of Mouse Hippocampal Neurons

Hippocampal neurons were isolated from fetuses (E18) of pregnant female *Ppara*-null and strain-matched WT littermate mice as described by us [6,30–32] with some modifications. Briefly, dissection and isolation procedures were performed in an ice-cold, sucrose buffer solution (sucrose 0.32 M, Tris 0.025 M; pH 7.4) [33]. The skin and the skull were carefully removed from the brain by scissors followed by peeling off the meninges by a pair of fine tweezers. Next, a fine incision was made in the middle line around the circle of Willis and medial temporal lobe was opened up. Hippocampus was isolated as a thin slice of tissue located near the cortical edge of medial temporal lobe. Hippocampal tissues isolated from all fetal pups (n >10) were combined together and homogenized with 1 ml of trypsin for 5 minutes at 37°C followed by neutralization of trypsin. The single cell suspension of hippocampal tissue was plated in the poly-D-lysine pre-coated 75 mm flask. Five min after plating, the supernatants were carefully removed and replaced with complete neurobasal media. The next day, 10 μM AraC was added to remove glial contamination in the neuronal culture. The pure cultures of hippocampal neurons were allowed to differentiate fully for 9–10 days before treatment [31,32,34].

Author Manuscript Author Manuscript Author Manuscript Author Manuscript

### Isolation of Mouse Astrocytes

Astrocytes were isolated from mixed glial cultures of 7 d old mouse pups according to the procedure of Guilian and Baker [35] as described earlier [7,36,37].

### Lentiviral cloning of *FL-Ppara* and mutated *Ppara*

**Site directed mutation—**The mouse PPARα ORF cloned in the pCMV6-AC-GFP vector (cat # MG 227641) was purchased from Origene. MG227641 was mutated at Tyr314 with aspartate (Y314D) and Tyr464 with aspartate (Y464D) by site-directed mutation kit (Stratagene)[6]. Two primers in opposite orientation were used to amplify the mutated plasmid in a single PCR reaction. The PCR product was precipitated with ethanol and then phosphorylated by T4 kinase. The phosphorylated fragment was self-ligated by T4 DNA ligase and digested with restriction enzyme DpnI to eliminate the non-mutated template. The mutated plasmid was cloned and amplified in Escherichia coli (DH5-a strain) competent cells.

**Generating pLenti6.3/V5-TOPO® constructs of FL-Ppara and mutated Ppara—**Briefly, each construct was amplified by PCR, using primer pair (sequence) and every product had a single adenosine (A) to the 3′ end. Then the TOPO cloning reaction was performed using the Invitrogen kit (K5315-20) with pLenti6.3/V5-TOPO vector. For transformation One-Shot Stbl3 competent cells were used. Sequencing of the clones was performed at ACGT Inc.

**Producing Lentivirus in 293FT Cells—**All protocols were approved by the Institutional Biosafety Committee (IBC #12092406) of the Rush University Medical Center. 293FT cells were cultured with 95% confluency in Opti-MEM media without antibiotics. Next day, ViraPower™ Packaging Mix (9 μg/reaction) and pLenti expression plasmid DNA containing either *FL-Ppara* or mutated *Ppara* (3 μg/reaction) (12 μg total) were mixed in 1.5 mL of serum-free Opti-MEM® I Medium. In another tube, 36 μL of Lipofectamine® 2000 was added in 1.5 mL of serum-free Opti-MEM® I Medium with gentle mix. After 5 minutes of incubation at room temperature, both the reactions were combined and incubated for 20 mins. After that, the mixture was applied to HEK-293FT cells and incubated overnight at 37°C in a humidified 5% $CO_2$ incubator. The next day, the media was replaced with serum-free Opti-MEM media and further incubated for 48–72 h at 37°C in a humidified 5% $CO_2$ incubator followed by collection of supernatants containing viral particles. Viral particles were concentrated with lenti-concentrator solution and MOI was calculated.

### Isolation of nuclear extracts and gas chromatography-mass spectra (GC-MS) analysis of PPARα-ligand interaction

**Sample preparation—**Either E18 cultured mouse hippocampal neurons or hippocampal tissues of 6–8 week old male C57/BL6J mice were homogenized in ice-cold nondetergent hypotonic buffer [10 mM HEPES (pH 7.9), 1.5 mM MgCl2, 10 mM KCl, 100 mM DTT, protease and phosphatase inhibitor cocktail]. After 10 min of additional incubation in the hypotonic buffer, the homogenate was centrifuged at 8,000 g at 4°C for 10 min. Next, the pellet was homogenized in ice-cold extraction buffer [10 mM HEPES (pH 7.9), 1.5 mM MgCl2, 0.21 M NaCl, 0.2 mM EDTA, 25% (v/v) glycerol, 100 mM DTT, protease and

Author Manuscript Author Manuscript Author Manuscript Author Manuscript

phosphatase inhibitor cocktail], placed on a rotating shaker at 4°C for 1 h, and then centrifuged at 18,000 g for 10 min. The supernatant (nuclear fraction) was incubated with 1.5 μg of GST PPARα LBD (Protein One) at 4°C for 6 h in a rotating shaker. The reaction mixture was passed through glutathione column (Pierce® GST Spin Purification Kit), washed four times [50 mM Tris HCl (pH 7.4), 100 mM NaCl, protease and phosphatase inhibitor cocktail] and then eluted with free glutathione. The eluate was transferred to methanol: chloroform: water (4:3:1) mixture and then centrifuged at 14,000 rpm for 90 sec. The organic phase was collected, evaporated in the SpeedVac, reconstituted with 30 μL chloroform or acetonitrile, and then analyzed by GC-MS. In another case, E18 cultured hippocampal neurons were transduced with lentiviral particles conjugated with PPARα-LBD or different GFP-tagged mutated constructs followed by pulling down with anti-PPARα antibody or passing the extract through GFP-column of Vector Fusion-Aid GFP Kit (Cat # MB-0732). After that, the eluate was collected from the column with 5M NaCl solution, concentrated with PD-10 desalting column and analyzed for GC-MS.

**GC-MS analyses—**A JEOL GCMate II (JEOL USA, Peabody MA) mass spectrometer was used in these experiments. The gas chromatograph was an Agilent 6890Plus (Wilmington DE) equipped with a G1513A auto-injector with 100 vial sample tray connected to a G1512A controller. The gas chromatography column was a fused silica capillary column with a nonpolar 5% phenyl 95% dimethylpolysiloxane phase (Agilent HP-5ms), 30 meters long, 0.25 mm internal diameter, 0.25 μm film thickness. The carrier gas was Helium (99.9995% Research Grade) run through a STG triple filter (Restek Corp.) at a constant flow rate 1.1 mL/min. The injector was held at 275°C and was fitted with an Agilent 4mm ID single taper split liner containing deactivated glass wool. One μL of solution was injected at a split ratio of 20:1. The initial oven temperature was 40°C held at 2 min, raised to 300°C at a rate of 10°C (Figure 2A–E) or 20°C (Figure 2K & 2L) per min, then held for 17 min (Figure 2A–E) or 30 min (Figure 2K & 2L). This explains the variable retention times of the identified compounds. Total run time was 45 min.

The mass spectrometer was a benchtop magnetic sector operating at a nominal resolving power of 500 using an accelerating voltage of 2500 volts. The spectrometer was operated in full scan EI mode (+Ve) with the filament operating at 70 eV scanning from m/z 10 to m/z 850 using a liner magnet scan. The scan speed was 0.3 sec per scan. The solvent delay was 4.0 min. Data analysis was performed using the TSS Pro software (Shrader analytical & Consulting Laboratories, Inc., Detroit MI) provided with the spectrometer. Reconstructed ion current (RIC) chromatographic peaks using ions unique to each compound were used for quantitation. Mass calibration was performed using perfluorokerosene (PFK).

### In Silico structural analyses of PPARα complexed with OCT, HEX and HMB

**Ligand Preparation—**Ligands (OCT, HEX and HMB) were subjected to LigPrep module implemented in Tripos software, which converted the 2D to 3D structure. Then using the ionization engine, the ligand was prepared at pH 7.0 ± 1. The appropriate stereoisomers were generated along with the low energetic conformers.

Author Manuscript Author Manuscript Author Manuscript Author Manuscript

**Protein Preparation—**The crystal structures for PPARα (3VI8.pdb), β (3GWX.pdb), and γ (3U9Q.pdb) were imported from the pdb databank. The protein preparation module of Tripos was utilized to fix up the hydrogen bonding orientation, bond orders, charges, missing side chain atoms, missing loop, protonation at physiological pH, and side chain bumps. Finally, staged minimization was performed for all three protein structures.

**Docking of the Ligands—**The Surflex docking module implemented in Tripos was used to carry out the docking of HEX, OCT and HMB in PPARα, β and γ crystal structures. After the docking, three major scoring functions such as Total Score (a function of $-\text{Log}K_d$), Crash Score (penalty score reflecting the inappropriate penetration of the ligand into the active site pocket) and Polar Score (depicting all the favorable polar interactions) were obtained.

We also computed the binding free energy of HEX, OCT and HMB in PPARα, using Molecular Mechanics Generalized Born Surface Area approach[38]. To account for the structural deformation upon binding, we included adaptation expense that accounts for changes in the intramolecular energetics ($\Delta G^0_{int}$). For ligand strain energy, we specified a 5å region of the receptor from the centroid of the ligand to be flexible so that the protein structure was relaxed in the computation of the binding energy of the ligands.

To soften the potential for the non-polar part of the ligands, the van der Waals radii of the atoms were scaled to 0.8 in a regular docking experiment. This allowed the dock pose to show as a successful pose even if the distance between the ligand atoms and the protein atoms are less than 1 Å away from each other. We increased the scaling factor to 1.2, in order to eliminate the unreasonable poses.

## TR-FRET analysis

TR-FRET assay was performed using Lanthascreen TR-FRET PPAR-alpha coactivator assay kit (Cat# PV4684) as described before[7]. Briefly, different doses of OCT, HEX and HMB were incubated with GST-tagged recombinant PPARα LBD protein, Terbium (Tb)-tagged anti GST antibody and Fluorescein (FL)-tagged PGC1α. The entire reaction was set up in corning 384-well plates using an automated robotic injector. Plate was centrifuged, incubated in a dark place for 30 min, and then analyzed “molecular devices analyst” machine equipped with dichroic mirror. The excitation wavelength and emission wavelength were set at 340 nm and 540 nm, respectively.

## Thermal shift assays

Thermal shift assays were performed in an Applied Biosystems 7500 standard real-time thermal cycler machine with commercially available thermal shift dye kit (Life technologies; Cat# 4461146) as described earlier[7]. For each reaction, purified protein (0.5 μg to 1μg) was added to 18 μL of thermal shift buffer provided with the kit, and 1–2μL of dye. Reaction was set 96 well PCR plate in the dark and then placed in the thermal cycler machine using the following two-stage program [(25°C for 2 mins) 1 cycle; (27°C for 15 sec, 26 °C for 1 min) 70 cycles; auto increment 1°C for both stages]. The filter was set at ROX with no quencher filter and no passive filter.

Author Manuscript Author Manuscript Author Manuscript Author Manuscript

### Microarray analyses

RNA samples were collected from hippocampal tissue of WT and Ppara-null (αKO) mice using Qiagen RNeasy kit (Cat# 74104). Quantity and purity of RNA were determined using the NanoDrop LTE (Nanodrop Technologies, Wilmington, DE, USA). The mRNA of each sample was converted into cDNA using SuperScript III First-Strand synthesis Kit (Thermofisher; Cat # 18080-051). Next, each cDNA sample was diluted at 1:2 ratio, mixed with SYBR Green qPCR Master Mix (Applied Biosystems, Cat # 4309155), and then aliquoted on 96 well Mouse Plasticity qPCR-arrays (SABiosciences; Cat #PAMM-126Z). Then 96-well plate was placed in ABI Prism 7500 standard qPCR System and run with stage 2, step 2 (60.0°C@1:00 min) "data collection" module. Once PCR is done, Ct values were imported from the PCR console and uploaded in SABiosciences website (http://pcrdataanalysis.sabiosciences.com/pcr/arrayanalysis.php) for further analyses. As recommended, we used online software modules to proceed with further calculations. Data normalization was performed by correcting all Ct values with the average Ct values of 12 constantly expressed housekeeping genes (HKGs) present on the array. PCR-array results were displayed by clustergram analyses with three color presentation from green (low expression) to black to red (high expression).

### RT-PCR analysis

Total RNA was digested with DNase and RT-PCR was carried out as described earlier[37,39] using a RT-PCR kit from Clontech. GAPDH (glyceraldehyde-3-phosphate dehydrogenase) was used to ascertain that an equivalent amount of cDNA was synthesized from different samples.

### Real-time PCR analysis

Real-time PCR analysis was performed in the ABI-Prism7700 sequence detection system (Applied Biosystems, Foster City, CA) as described earlier[37,39] using TaqMan Universal Master mix and FAM-labeled probes and primers (Applied Biosystems). Data were processed by the ABI Sequence Detection System 1.6 software and analyzed by ANOVA.

### Immunoblot analysis

For whole-cell and tissue lysates, samples were homogenized in RIPA buffer containing protease and phosphatase inhibitors (Sigma), passed 10 times through a 26-gauge needle, rotated end over end for 30 min at 4°C, and centrifuged for 10 min at 18,000 × g. The supernatant was aliquoted and stored at 80°C until use. Protein concentrations were determined using a NanoDrop 2000 (Thermo Fisher), and 15–30 μg sample was heat-denatured and resolved on 10% or 12% polyacrylamide-SDS gels, transferred to 0.45 μm nitrocellulose membranes under semidry conditions (15V for 12 min). Membranes were blocked for 1 h with blocking buffer (Li-Cor), incubated with primary antibodies overnight at 4°C under shaking conditions, washed, incubated with IR-dye-labeled secondary antibodies (1:17,000; Li-Cor) for 45 min at room temperature, washed, and visualized with the Odyssey Infrared Imaging System (Li-Cor). Blots were converted to grayscale and then binary, analyzed using Fiji, and normalized to appropriate loading controls.

Author Manuscript Author Manuscript Author Manuscript Author Manuscript

### Immunohistochemical analysis

Hippocampal neurons were transduced with GFP-containing lentivirions for 2 d. Neurons were stained with Dylight-554-conjugated phalloidin (Cat# 21834; Thermo Fisher) as per manufactures protocol and visualized in fluorescence microscope. For tissue staining, 10 μm paraffin embedded mouse brain hippocampal sections were made from 8- to10-week-old male WT and *Ppara*-null mice and immuno-stained with anti-PPARα and anti-NeuN antibodies.

### Statistical analyses

All values are expressed as the mean ± SD. Differences among means were analyzed using one- or two-way ANOVA with dose of ligands or genotype as the independent factors using SPSS. Homogeneity of variance between test groups was examined using Levene's test. *Post-hoc* analyses of between-subjects effects were conducted using Scheffe's, Tukey's or Games-Howell tests, where appropriate. $p < 0.05$ was considered statistically significant.

## Supplementary Material

Refer to Web version on PubMed Central for supplementary material.

## Acknowledgments

This study was supported by grants from NIH (AG050431 and NS83054) and a merit award (1I01BX003033-01) from Veterans Affairs. The authors would like to thank ChemCore at the Center for Molecular Innovation and Drug Discovery, Northwestern University, funded by the Chicago Biomedical Consortium.

## References

1. Issemann I, Green S. Activation of a member of the steroid hormone receptor superfamily by peroxisome proliferators. Nature. 1990; 347:645–50. [PubMed: 2129546]
2. Keller H, et al. Fatty acids and retinoids control lipid metabolism through activation of peroxisome proliferator-activated receptor-retinoid X receptor heterodimers. Proc Natl Acad Sci U S A. 1993; 90:2160–4. [PubMed: 8384714]
3. Lehmann JM, Lenhard JM, Oliver BB, Ringold GM, Kliewer SA. Peroxisome proliferator-activated receptors alpha and gamma are activated by indomethacin and other non-steroidal anti-inflammatory drugs. J Biol Chem. 1997; 272:3406–10. [PubMed: 9013583]
4. Gocke AR, et al. Transcriptional modulation of the immune response by peroxisome proliferator-activated receptor-{alpha} agonists in autoimmune disease. J Immunol. 2009; 182:4479–87. [PubMed: 19299749]
5. Cabrero A, et al. Increased reactive oxygen species production down-regulates peroxisome proliferator-activated alpha pathway in C2C12 skeletal muscle cells. J Biol Chem. 2002; 277:10100–7. [PubMed: 11792699]
6. Roy A, et al. Regulation of cyclic AMP response element binding and hippocampal plasticity-related genes by peroxisome proliferator-activated receptor alpha. Cell Rep. 2013; 4:724–37. [PubMed: 23972989]
7. Roy A, et al. HMG-CoA Reductase Inhibitors Bind to PPARalpha to Upregulate Neurotrophin Expression in the Brain and Improve Memory in Mice. Cell Metab. 2015; 22:253–265. [PubMed: 26118928]
8. Roy A, Pahan K. PPARalpha signaling in the hippocampus: crosstalk between fat and memory. J Neuroimmune Pharmacol. 2015; 10:30–4. [PubMed: 25575492]

Author Manuscript Author Manuscript Author Manuscript Author Manuscript


9. Corbett GT, Gonzalez FJ, Pahan K. Activation of peroxisome proliferator-activated receptor alpha stimulates ADAM10-mediated proteolysis of APP. Proc Natl Acad Sci U S A. 2015; 112:8445–50. [PubMed: 26080426]
10. Fanelli F, et al. Age-dependent roles of peroxisomes in the hippocampus of a transgenic mouse model of Alzheimer's disease. Mol Neurodegener. 2013; 8:8. [PubMed: 23374228]
11. Gronemeyer H, Gustafsson JA, Laudet V. Principles for modulation of the nuclear receptor superfamily. Nat Rev Drug Discov. 2004; 3:950–64. [PubMed: 15520817]
12. Campolongo P, et al. Fat-induced satiety factor oleoylethanolamide enhances memory consolidation. Proc Natl Acad Sci U S A. 2009; 106:8027–31. [PubMed: 19416833]
13. Fu J, Oveisi F, Gaetani S, Lin E, Piomelli D. Oleoylethanolamide, an endogenous PPAR-alpha agonist, lowers body weight and hyperlipidemia in obese rats. Neuropharmacology. 2005; 48:1147–53. [PubMed: 15910890]
14. LoVerme J, La Rana G, Russo R, Calignano A, Piomelli D. The search for the palmitoylethanolamide receptor. Life Sci. 2005; 77:1685–98. [PubMed: 15963531]
15. Fang X, et al. 20-carboxy-arachidonic acid is a dual activator of peroxisome proliferator-activated receptors alpha and gamma. Prostaglandins Other Lipid Mediat. 2007; 82:175–84. [PubMed: 17164145]
16. Narala VR, et al. Leukotriene B4 is a physiologically relevant endogenous peroxisome proliferator-activated receptor-alpha agonist. J Biol Chem. 2010; 285:22067–74. [PubMed: 20400503]
17. Chen L, et al. Oleoylethanolamide, an endogenous PPAR-alpha ligand, attenuates liver fibrosis targeting hepatic stellate cells. Oncotarget. 2015; 6:42530–40. [PubMed: 26729705]
18. Mattace Raso G, et al. N-Palmitoylethanolamide protects the kidney from hypertensive injury in spontaneously hypertensive rats via inhibition of oxidative stress. Pharmacol Res. 2013; 76:67–76. [PubMed: 23917217]
19. Melis M, Carta G, Pistis M, Banni S. Physiological role of peroxisome proliferator-activated receptors type alpha on dopamine systems. CNS Neurol Disord Drug Targets. 2013; 12:70–7. [PubMed: 23394525]
20. Chakravarthy MV, et al. Identification of a physiologically relevant endogenous ligand for PPARalpha in liver. Cell. 2009; 138:476–88. [PubMed: 19646743]
21. Kauer JA, Malenka RC, Nicoll RA. NMDA application potentiates synaptic transmission in the hippocampus. Nature. 1988; 334:250–2. [PubMed: 2840582]
22. Mulkey RM, Herron CE, Malenka RC. An essential role for protein phosphatases in hippocampal long-term depression. Science. 1993; 261:1051–5. [PubMed: 8394601]
23. Harris KM, Jensen FE, Tsao B. Three-dimensional structure of dendritic spines and synapses in rat hippocampus (CA1) at postnatal day 15 and adult ages: implications for the maturation of synaptic physiology and long-term potentiation. J Neurosci. 1992; 12:2685–705. [PubMed: 1613552]
24. Roy A, et al. Enhancement of morphological plasticity in hippocampal neurons by a physically modified saline via phosphatidylinositol-3 kinase. PLoS One. 9:e101883.
25. Kainu T, Wikstrom AC, Gustafsson JA, Pelto-Huikko M. Localization of the peroxisome proliferator-activated receptor in the brain. Neuroreport. 1994; 5:2481–5. [PubMed: 7696585]
26. Chakravarthy MV, et al. Brain fatty acid synthase activates PPARalpha to maintain energy homeostasis. J Clin Invest. 2007; 117:2539–52. [PubMed: 17694178]
27. Fu J, et al. Oleylethanolamide regulates feeding and body weight through activation of the nuclear receptor PPAR-alpha. Nature. 2003; 425:90–3. [PubMed: 12955147]
28. Cluny NL, Keenan CM, Lutz B, Piomelli D, Sharkey KA. The identification of peroxisome proliferator-activated receptor alpha-independent effects of oleoylethanolamide on intestinal transit in mice. Neurogastroenterol Motil. 2009; 21:420–9. [PubMed: 19140957]
29. Huitron-Resendiz S, Gombart L, Cravatt BF, Henriksen SJ. Effect of oleamide on sleep and its relationship to blood pressure, body temperature, and locomotor activity in rats. Exp Neurol. 2001; 172:235–43. [PubMed: 11681856]
30. Roy A, et al. Enhancement of morphological plasticity in hippocampal neurons by a physically modified saline via phosphatidylinositol-3 kinase. PLoS One. 2014; 9:e101883. [PubMed: 25007337]

Author Manuscript Author Manuscript Author Manuscript Author Manuscript

31. Jana M, Jana A, Pal U, Pahan K. A simplified method for isolating highly purified neurons, oligodendrocytes, astrocytes, and microglia from the same human fetal brain tissue. Neurochem Res. 2007; 32:2015–22. [PubMed: 17447141]
32. Saha RN, et al. TNF-alpha preconditioning protects neurons via neuron-specific up-regulation of CREB-binding protein. J Immunol. 2009; 183:2068–78. [PubMed: 19596989]
33. Gorini A, D'Angelo A, Villa RF. Energy metabolism of synaptosomal subpopulations from different neuronal systems of rat hippocampus: effect of L-acetylcarnitine administration in vivo. Neurochem Res. 1999; 24:617–24. [PubMed: 10344589]
34. Saha RN, Pahan K. Differential regulation of Mn-superoxide dismutase in neurons and astroglia by HIV-1 gp120: Implications for HIV-associated dementia. Free Radic Biol Med. 2007; 42:1866–78. [PubMed: 17512466]
35. Giulian D, Baker TJ. Characterization of ameboid microglia isolated from developing mammalian brain. J Neurosci. 1986; 6:2163–78. [PubMed: 3018187]
36. Dasgupta S, Jana M, Liu X, Pahan K. Role of very-late antigen-4 (VLA-4) in myelin basic protein-primed T cell contact-induced expression of proinflammatory cytokines in microglial cells. J Biol Chem. 2003; 278:22424–31. [PubMed: 12690109]
37. Roy A, Fung YK, Liu X, Pahan K. Up-regulation of microglial CD11b expression by nitric oxide. J Biol Chem. 2006; 281:14971–80. [PubMed: 16551637]
38. Im W, Feig M, Brooks CL 3rd. An implicit membrane generalized born theory for the study of structure, stability, and interactions of membrane proteins. Biophys J. 2003; 85:2900–18. [PubMed: 14581194]
39. Ghosh A, et al. Selective inhibition of NF-kappaB activation prevents dopaminergic neuronal loss in a mouse model of Parkinson's disease. Proc Natl Acad Sci U S A. 2007; 104:18754–9. [PubMed: 18000063]

Author Manuscript Author Manuscript Author Manuscript Author Manuscript

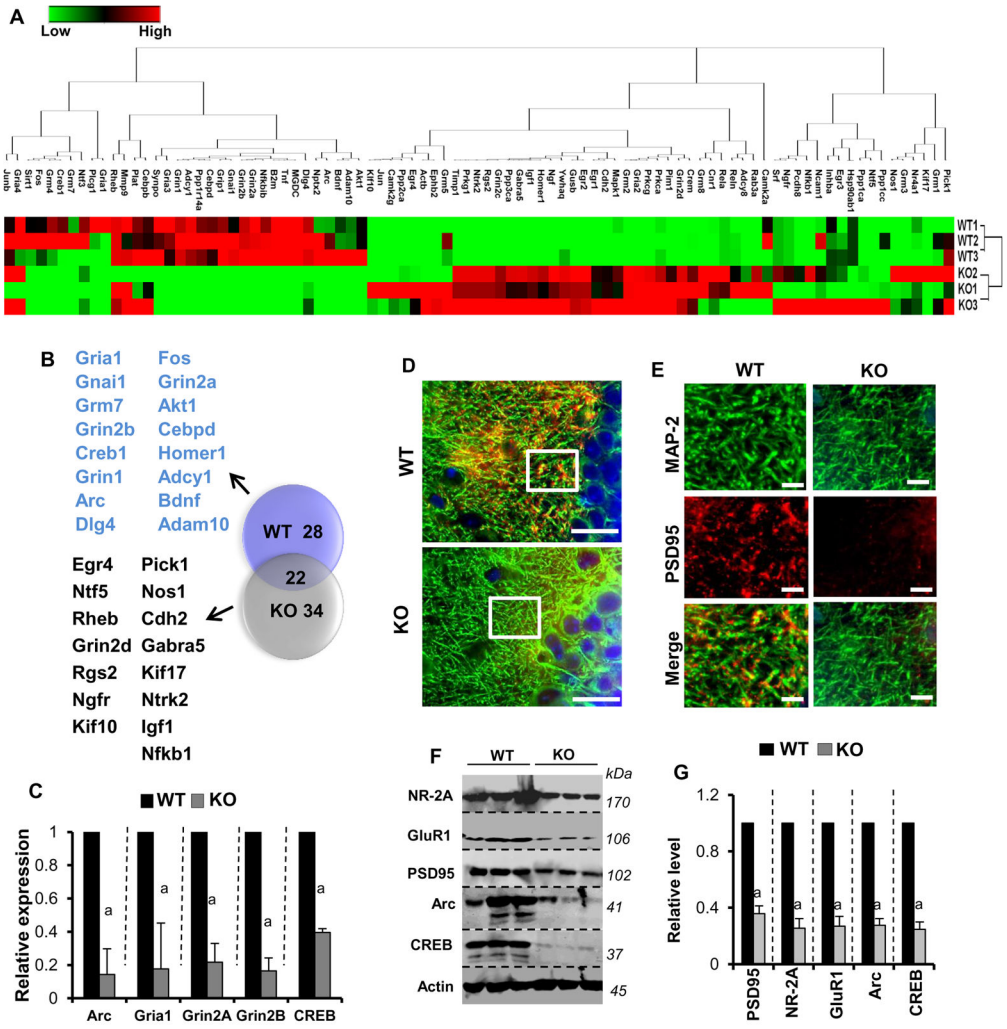


**Figure 1. PPARα is critical in regulating the expression of synaptic molecules in hippocampal neurons**

A) Heat map analysis shows the PCR-based microarray analysis of plasticity-associated genes in the hippocampus of WT and αKO (*Ppara*-null) mice. Three mice were used in each group. B) Venn diagram of plasticity-associated genes shows the number of genes inhibited (28; red circle), stimulated (34; green circle) and unchanged (22; overlapped region) in *Ppara*-null hippocampus. C) Real-time PCR analyses of *Arc, Creb, Grin2a, Grin2b,* and *Gria1* mRNAs were performed to confirm the array results. Results are mean ± SEM of three mice. [a]*p<0.001 vs WT*. D) Hippocampal tissue of 6- to 8-week-old WT (n=3) and *Ppara*-null (n=3) mice were immunostained for MAP-2 (green) and PSD-95 (red). The representative image was taken from CA1 region of the hippocampus. Scale bar = 10μm. E) The magnified view of region enclosed in the box is shown in the image. Scale bar = 10 μm. Results represent analysis of three hippocampal sections of each of three mice per group. The expression of NR-2A, GluR1, PSD95, Arc, and CREB in hippocampal tissue of WT (*n=3*) and *Ppara*-null (*n=3*) mice was further assessed by Western blot (F) followed by

Author Manuscript Author Manuscript Author Manuscript Author Manuscript

densitometric analyses (G) after normalizing with actin. For raw uncut blots, please see Supplementary Figure 13A. Results are mean ± SEM of three mice. [a]*p<0.001 vs WT*.

Author Manuscript Author Manuscript Author Manuscript Author Manuscript

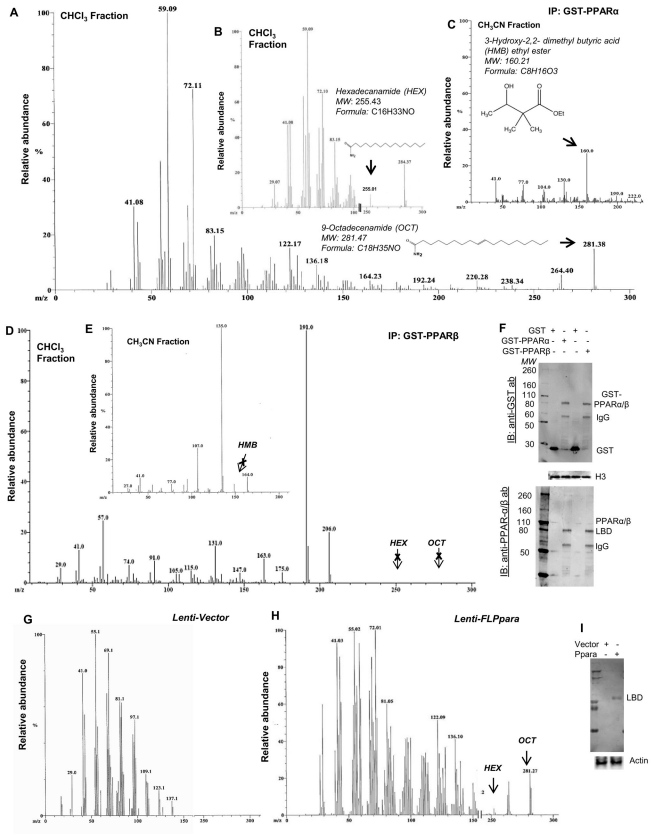


**Figure 2. Identification of endogenous iigands of PPARα in the mouse brain hippocampus**

GC-MS analyses of chloroform- (A & B) and acetonitrile- (C) reconstituted nuclear extracts of WT hippocampus after pulling down with GST-PPARα-LBD. Similar GC-MS analyses were performed in chloroform (D) and acetonitrile (E) reconstituted nuclear extracts after pulling down with GST-PPARβ-LBD. F) The immunoblot analyses of eluate collected from glutathione column probed with anti-GST antibody (upper panel), and anti-PPARα or anti-PPARβ antibodies (lower panel). Histone 3 (H3) immunoblot was performed in the nuclear lysate (input) to show the purity of the nuclear extract (middle panel). For raw uncut blots, please see Supplementary Figure 13B. GC-MS analyses of the chloroform-extracted nuclear fraction of lenti-vector- (G) and lenti-PPARα- (H) transduced *Ppara*-null hippocampal neurons. I) Neuronal extracts infected with lenti-vector and lenti-PPARα were analyzed for PPARα and then normalized with actin. For raw uncut blots, please see Supplementary Figure 13C. Results were confirmed by three independent experiments.

Author Manuscript Author Manuscript Author Manuscript Author Manuscript

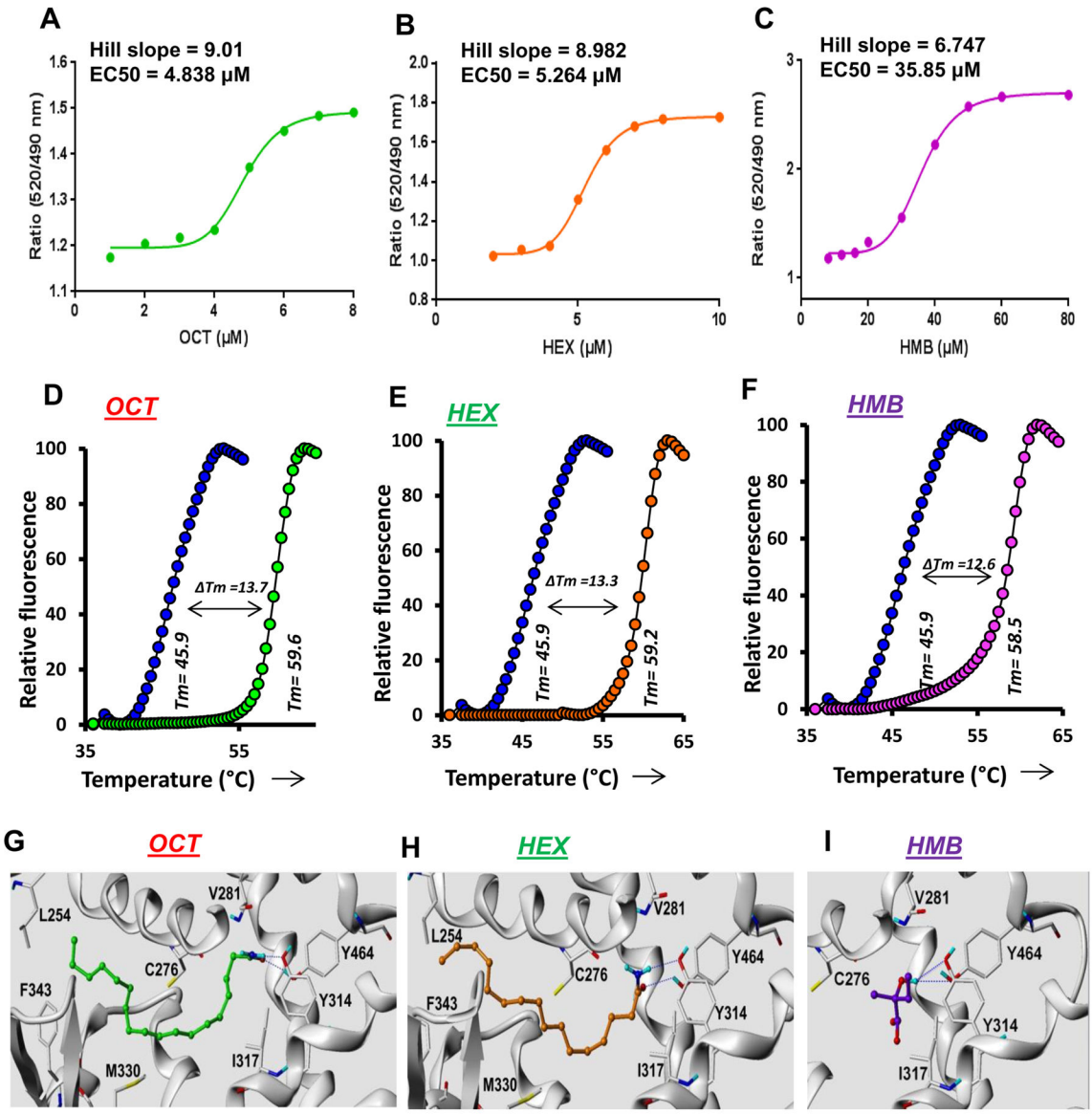


**Figure 3. Analyses of the interaction of OCT, HEX and HMB with PPARα by TR-FRET and thermal shift**

TR-FRET analyses were performed and fitted curves are shown for OCT (A), HEX (B) and HMB (C). Dose response curves were plotted as a ratio of fluorescence response with increasing doses of agonists. Graph-pad prism 7 software was used to draw a sigmoidal curve-fit. Respective EC50 (4.838 µM for OCT, 5.264 µM for HEX and 35.85 µM for HMB) and hill slope (9.01 for OCT, 8.982 for HEX and 6.747 for HMB) values were calculated based on sigmoidal curve-fit equation: Y=Bottom + ($X^{Hillslope}$)*(Top-Bottom)/($X^{Hillslope}$ + $EC50^{Hillslope}$). Thermal-shift assay of OCT (D), HEX (E) and HMB (F) was performed using 5 µM OCT, 5 µM HEX and 25 µM HMB as described under the Materials and Method section.

Equation for full-length protein only:

Author Manuscript Author Manuscript Author Manuscript Author Manuscript

$$y=50=-0.0652x^3+9.053x^2-408.09x+6012.7;\ x=45.96321$$

Equation for full length protein with OCT:

$$y=50=-0.0002x^5+0.052x^4-5.1349x^3+250.52x^2-6041.9x+57653;\ x=59.6128$$

Equation for full length protein with HEX:

$$y=0.0074x^3-0.8528x^2+31.967x-389.74;\ x=59.2835$$

Equation for full length protein with HMB:

$$y=-0.06529x^3+9.053x^2-408.09x+6012.7;\ x=58.494798$$

Ribbon representations of superposed structures of PPARα ligand binding pocket along with its ligands OCT (G), HEX (H) and HMB (I) are shown. Blue dotted lines represent potential hydrogen bonds. Results are confirmed by three independent experiments.

Author Manuscript Author Manuscript Author Manuscript Author Manuscript

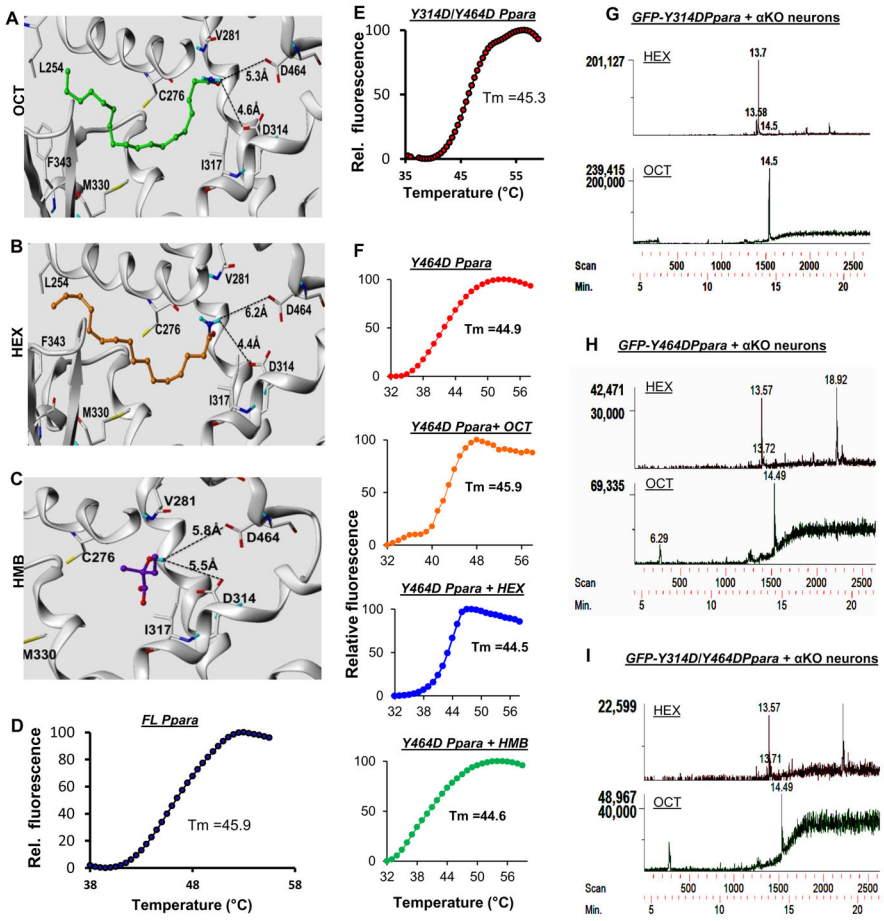


**Figure 4. Interaction between ligands and PPARα at the molecular level**

Ribbon representations of superposed structures of Y464D/Y314D-PPARα ligand binding pocket along with OCT (A), HEX (B) and HMB (C). Thermal shift assays of FL-PPARα (D) and Y314D/Y464D-PPARα (E) proteins. Tm represents the melting temperature. F) Thermal shift assay for Y464D-PPARα alone and together with three ligands. GC-MS analyses in GFP-affinity purified extracts of *Ppara*-null hippocampal neurons transduced with lentivirions containing *GFP-Y314D-Ppara* (G), *GFP-Y464D-Ppara* (H), and *GFP-Y314D/Y464D-Ppara* (I).

Author Manuscript Author Manuscript Author Manuscript Author Manuscript

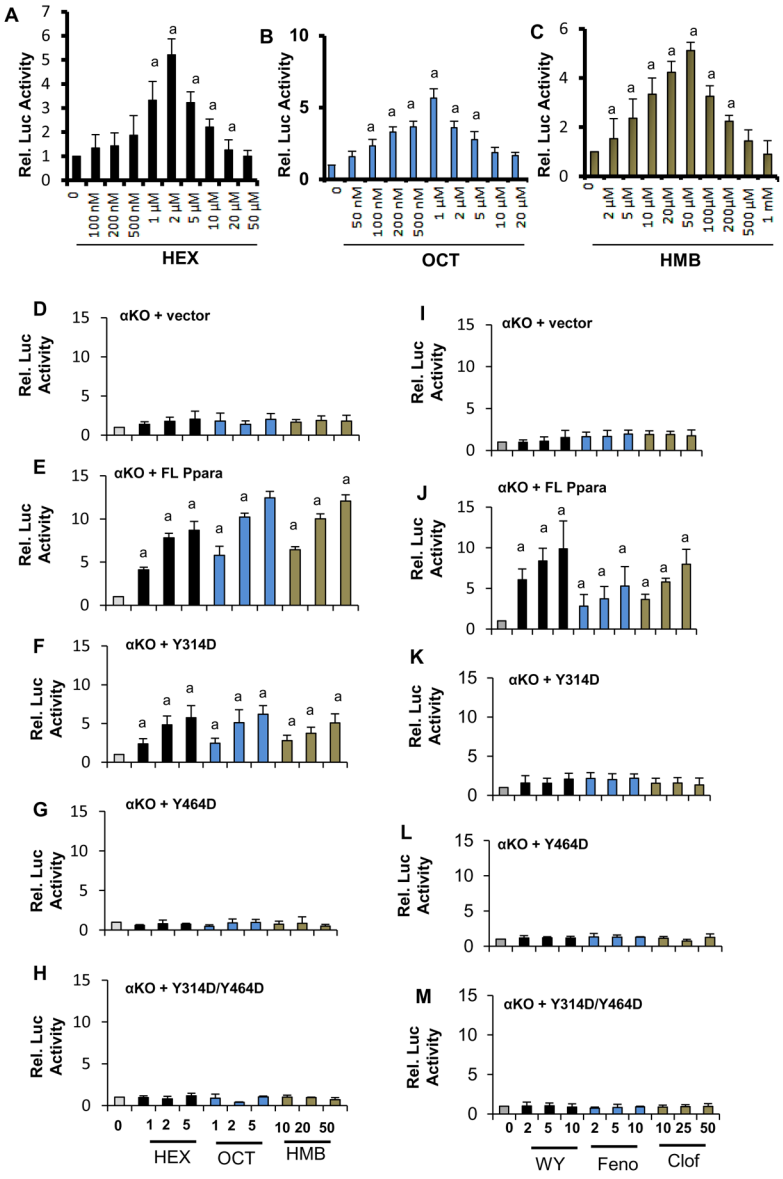


**Figure 5. Hippocampal ligands of PPARα induce PPRE-driven luciferase activity in primary mouse astrocytes and neurons**

Astrocytes plated at 60–70% confluence were transfected with *tk-PPREx3-Luc*, a PPRE-dependent luciferase reporter construct. After 24 h of transfection, cells were treated with different concentrations of HEX (A), OCT (B) and HMB (C) for 4 h followed by monitoring luciferase activity. Results are mean ± SD of three independent experiments. $^{a}p< 0.001$ *vs. control. Ppara*-null astrocytes were transduced with lentivirions containing empty vector (D), *FL-Ppara* (E), *Y314D-Ppara* (F), *Y464D-Ppara* (G), and *Y314D/Y464D-Ppara* (H) for 48 h followed by transfection with *tk-PPREx3-Luc*. After 24 h of transfection, cells were treated with different doses of HEX, OCT and HMB for 4 h followed by monitoring luciferase activity. PPRE luciferase activity was assayed in *Ppara*-null astrocytes transduced with lentivirions containing empty vector (I), *FL-Ppara* (J), *Y314D-Ppara* (K), *Y464D-Ppara* (L),

Author Manuscript Author Manuscript Author Manuscript Author Manuscript

and *Y314D/Y464D-Ppara* (M) after treatment with different doses of WY14643, fenofibrate, and clofibrate. Results are mean ± SD of three independent experiments. [a]*p< 0.001 vs. control.*

Author Manuscript Author Manuscript Author Manuscript Author Manuscript

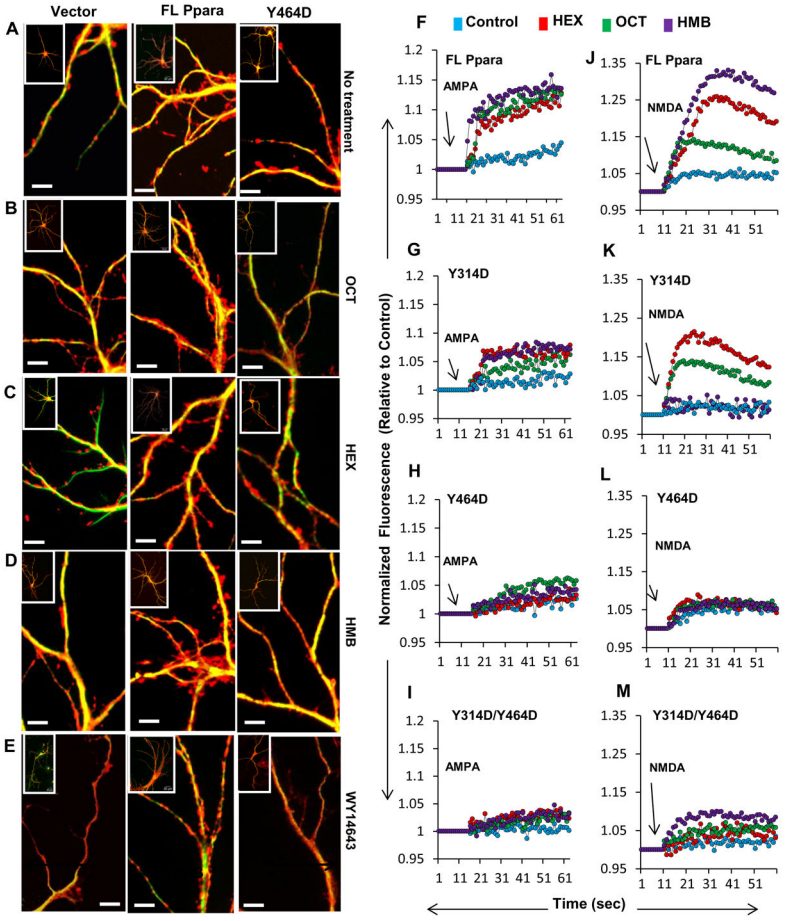


**Figure 6. Effect of hippocampal ligands of PPARα on morphological plasticity and calcium oscillation in hippocampal neurons**

*Ppara*-null hippocampal neurons were transduced with lentivirions containing GFP (vector), *FL-Ppara*, and *Y464D-Ppara* for 48 h followed by treatment with vehicle (DMSO) (A), OCT (B), HEX (C), HMB (D), and WY14643 (E) for 24 h. Then neurons were stained for phalloidin to measure spine density. Scale bar = 20 μm. AMPA-driven calcium influx was measured in OCT (red), HEX (green) and HMB (purple)-treated *Ppara*-null hippocampal neurons transduced with lentivirions containing *FL-Ppara* (F), *Y314D-Ppara* (G), *Y464D-Ppara* (H), and *Y314D/Y464D-Ppara* (I). All neurons were treated with 50 μM of NMDA receptor antagonist N20C to inhibit passive calcium flow through NMDA receptor. (J–M) Similarly NMDA-driven calcium influx was measured in the lentivius-infected *Ppara*-null hippocampal neurons in the presence of different endogenous ligands. In these cases, Naspm-HCl was treated to stop the passive flow of calcium currents through AMPA receptor. Results are mean of three independent experiments.